MRAS rotor resistance estimators for EV vector controlled induction motor traction drive: Analysis and experimental results

F.L. Mapelli *, D. Tarsitano, F. Cheli

Department of Mechanical Engineering, Politecnico di Milano, via G. La Masa 1, 20156 Milano, Italy

The Field Oriented Control algorithm needs accurate estimation of motor state variables in order to ensure full torque performances and good efficiency. On electric vehicle traction drives, Induction motor Field Oriented Control is widely adopted. Good control results are strongly related to parameter values used by observers or estimators, which vary according to machine working conditions and temperature. The most important parameter is the rotor resistance. The paper shows and compares two different MRAS rotor resistance estimators, based on reactive power and motor torque, studied by means of a sensitivity analysis for different load and speed operating conditions. A nonlinear correction algorithm has been pro-posed in order to assure a good rotor resistance estimation convergence also under dynamic conditions. Sensitivity analysis, simulation and experimental results are reported for the proposed methods. The esti-mation algorithm has been also experimentally tested on a prototypal electric vehicle to demonstrate its validity under dynamic condition during a real driving cycle.

Keywords: Adaptive algorithm, Full electric vehicle, On-line rotor resistance estimation MRAS approach, Induction motor, Field Oriented Control, Sensitivity analysis

1. Introduction

Induction motors are widely used in railway [1] and in Electrical Vehicles (EV) [2–4,5] traction applications because of their simplicity, robustness, reliability and low cost. The IM-based electrical drives for electric vehicles are usually controlled according to the Field Oriented Control (FOC) technique [6–8], which allows to control the torque by means of flux and current regulation [5]. In Fig. 1 the overall block diagram of the rotor flux sensored FOC scheme for an IM is presented. This classic control scheme has been chosen for its robustness and for its capability to work in field weakening conditions. Since some of the quantities reported in the control scheme are not directly measurable, observers or estimators are needed. In order to work properly, these algorithms require the value of some motor parameters, which often cannot be exactly identified and may vary during the operation, especially because of motor temperature fluctuations. In EVs the control algorithm has to assure the capability to exploit the maximum torque in the whole speed range, a weak dependence on the motor parameters, achieve the maximum efficiency and a stable and smooth driving performance. The most critical parameter is the rotor resistance, because the effectiveness of the control is strictly related to it, as well explained in Ref. [9]. If the estimated value is different from the real one, low efficiency and low torque per ampere are obtained because of the misalignment in flux position estimation/observation.

For an electric vehicle, since torque performance and efficiency are the most important factors, the proper estimation of rotor resistance assures good torque performances and efficiency. Therefore, in order to ensure full motor performances, the rotor resistance has to be estimated continuously. Different observers, such as full-order state observers [10,11], extended Kalman filters [12–14], Model Reference Adaptive System (MRAS)-based estimators [15–21] and neural networks [22,23] are proposed in literature. The main drawback of many of these algorithms is that they require a high performance hardware to compute the estimated values, since they need to solve complex non-linear equations. Furthermore, the accuracy and the stability of these algorithms are often demonstrated in steady-state or in linearized conditions, which implies that the motor works around an equilibrium point. This is not the most common working condition for an EV motor, since the road conditions and the variable driver requests never permit to operate in steady state for a long time. The present paper proposes a simple estimation and correction algorithm easy to implement on an industrial motor control hardware system (DSP or microcontroller) with a low computation load. This algorithm is able to on-line calculate the IM rotor resistance value under dynamic working conditions. In order to define this algorithm, two different

Article history:
Received 27 July 2015
Received in revised form
23 December 2016
Accepted 8 February 2017

* Corresponding author.
E-mail addresses: ferdinando.mapelli@polimi.it (F.L. Mapelli), davide.tarsitaano@polimi.it (D. Tarsitano), federico.cheli@polimi.it (F. Cheli).

Published Journal Article available at: http://dx.doi.org/10.1016/j.epsr.2017.02.005

Nomenclature

d,q	Rotating reference frame
e_x	Error between real and estimated value of the generic variable x
i_s	Stator current
j	Imaginary unit
L_{ks}	Total leakage inductance
M	Mutual inductance
n	Pole-pairs number
p	Derivative symbol
Q	Motor reactive power
R_s	Stator resistance
R_r	Rotor resistance
$\hat{R}_r$	Estimated rotor resistance
T	Torque
v_s	Stator voltage
$_s$	Stator flux
$_r$	Rotor flux
α,β	Stationary reference frame
γ	Angle between the stator current and the rotor flux space vectors
ΔR_r	Error between estimated and real rotor resistance
$\dot{\theta}_s$	Reference frame angular speed (synchronism speed)
$\dot{\theta}$	Mechanical angular speed (at magnetic field)
Ω_m	Mechanical angular speed (at shaft, $\Omega_m = \dot{\theta}/n$)
$\dot{\theta}_r$	Absolute rotor slip speed ($\dot{\theta}_r = \dot{\theta}_s - \dot{\theta}$)
$\Im(\bar{h})$	Imaginary part of a generic complex number $\bar{h}$

MRAS rotor resistance indicators (also called errors), based respectively on reactive power and motor torque, have been analyzed and relations between the rotor resistance value and the motor load conditions (torque, slip and speed) have been expressed [24]. The sensitivity analysis, conducted on these indicators, allows to find a set of working conditions under which all the methods have a similar behavior, which have been used as guidelines to identify the rotor resistance estimation and correction algorithm. In the following sections the motor model, the rotor flux estimator and the two MRAS systems will be presented. Furthermore, simulated and experimental results of the on-line implementation of the correction algorithm will be presented in order to verify that the proposed MRAS methods provide a correct estimation under dynamic conditions. In the last part of the present paper, an experimental validation test in the real field application condition (i.e. in the implementation on an electric vehicle) is shown. The validation experiment has been performed while the vehicle was covering an urban drive cycle. In the scientific literature, the experimental validation is, in most cases,performed on test benches and not on a real field application.

2. IM model and FOC scheme

The dynamic model of an IM in a rotating d-q reference frame synchronous with rotor flux space vector, assuming the rotor flux vector oriented as the d axis, is given by (1) [25,26].

$$\begin{cases} v_{sd} = (R_s + R_r)\, i_{sd} + L_{ks} p i_{sd} - \dot{\theta}_s L_{ks} i_{sq} - \dfrac{R_r}{M}\ {}_r \\ v_{sq} = (R_s + R_r)\, i_{sq} + L_{ks} p i_{sq} + \dot{\theta}_s L_{ks} i_{sd} + \dot{\theta}\ {}_r \\ p\psi_r = R_r \left(i_{sd} - \dfrac{r}{M} \right) \\ 0 = R_r i_{sq} - \dot{\theta}_r \psi_r \\ T = n \psi_r i_{sq} = n \psi_r i_s \sin\gamma \end{cases} \tag{1}$$

Since the rotor flux vector $\bar{\psi}_r$ cannot be directly measured, a flux estimator is needed. From the third and the fourth equation of (1), the simple estimator reported in (2) can be obtained [6], where quantities with hat ($\hat{x}$) are the estimated values of generic variables or parameters (x).

$$\begin{cases} p\hat{\psi}_r = \hat{R}_r \left(i_{sd} - \dfrac{\hat{\psi}_r}{M} \right) \rightarrow \hat{\psi}_r \\ \hat{\theta}_s = \hat{R}_r \dfrac{i_{sq}}{\hat{\psi}_r} + \dot{\theta} \rightarrow \hat{\theta}_s \end{cases} \tag{2}$$

The estimator reported in (2) clearly shows that the magnitude and the position of the estimated rotor flux phasor depend on the R_r value (M is assumed to be well-known). Therefore, if the $\hat{R}_r$ value used in the estimator differs from the real one, a wrong d-q axes position estimation is obtained, as shown in Fig. 2.

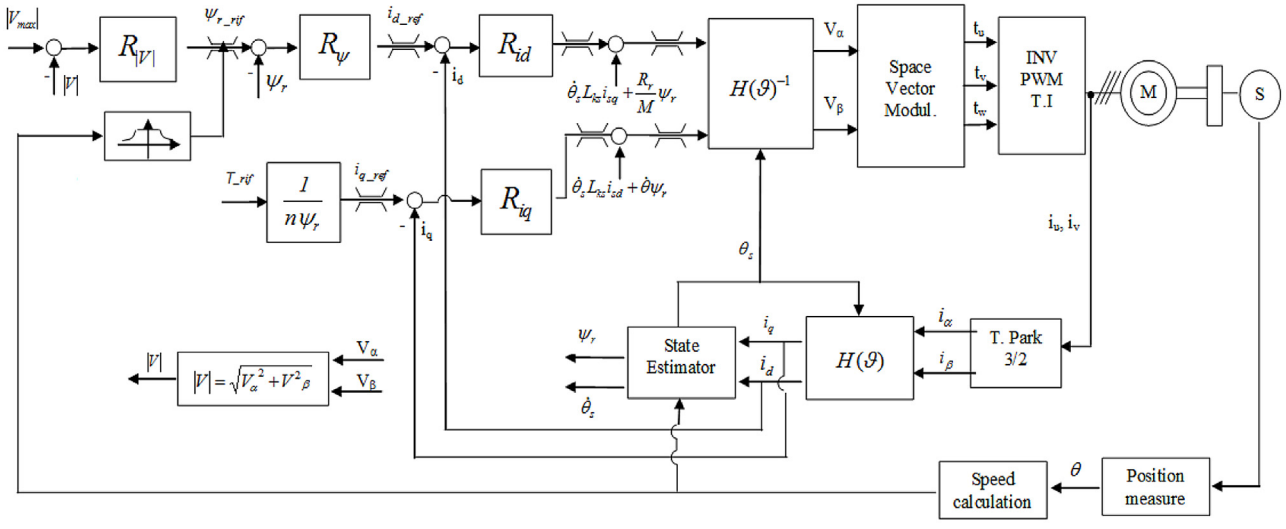

Fig. 1. Sensored Field Oriented Control scheme for an Induction Motor on EV.

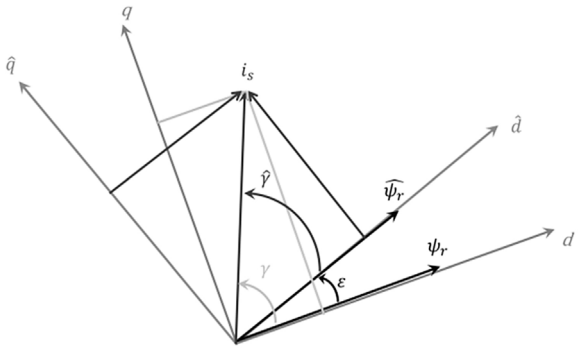

Fig. 2. Effect of wrong flux estimation on reference frames ($\hat{R}_r \neq R_r$).

The control scheme reported in Fig. 1 is based on the motor model (1), where the stator current is split in two components, respectively used to produce the machine flux and the torque.

It is possible to notice that the accuracy of the control depends on the correctness of the decoupling terms for the regulators and on the switching commands generated for the power stage, which are all related to the estimation algorithm outputs (see Fig. 1). Since this stage is influenced by the time-varying motor parameters, in particular by R_r, an online estimation is needed.

3. MRAS approach

To adjust the R_r value used in the estimator, a MRAS technique has been adopted. According to this method, an error indicator can be obtained using the difference between the outputs of two dynamic models. These models are named respectively "reference model", which is independent from uncertain model parameters, and "adjustable model" which is instead dependent on parameters. They are fed by the same inputs, so that any difference between output values of the two models is related to wrong parameters in the adjustable model. This error can be used to drive a correction algorithm.

The proposed algorithms for parameter $\hat{R}_r$ are based on two error indicators:

$$e_T = T - \hat{T} \tag{3}$$

$$e_Q = Q - \hat{Q} \tag{4}$$

named respectively torque and reactive power error. According to the MRAS approach, reference models are shown in (5) and (6).

$$T = \psi_{s\alpha} i_{s\beta} - \psi_{s\beta} i_{s\alpha} \tag{5}$$

$$Q = v_{s\beta} i_{s\alpha} - v_{s\alpha} i_{s\beta} \tag{6}$$

It is possible to notice that reference models are based on fluxes, voltages and currents referred to a stationary α, β reference frame. Stator currents are easily measured and stator voltages are easily reconstructed using the PWM reference and DC-link voltage measurement. In particular, the stator flux is obtained from stator voltages and currents according to (7), in which a first-order low-pass filter is adopted instead of the pure integrator for stability purpose.

$$_{s\alpha,\beta} = \int (v_{s\alpha,\beta} - R_s i_{s\alpha,\beta}) dt \tag{7}$$

Adjustable models are shown in (8) and (9), where the symbol $\bar{i}^s$ indicates the complex conjugate quantity of $\bar{i}_s$.

$$\hat{T} = n \hat{\psi}_r \hat{i}_{sq} \tag{8}$$

Table 1
Motor parameters (in [p.u.]).

Parameter	Values
Rotor resistance R_r	0.0221
Stator resistance R_s	0.0284
Mutual inductance M	2.4712
Total leakage inductance L_{ks}	0.2896

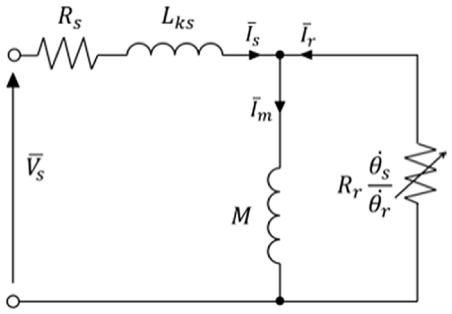

Fig. 3. Steady state model for IM.

$$\begin{aligned} \hat{Q} &= \Im(\bar{\hat{v}}_s \cdot \bar{\hat{i}}^s) = \hat{v}_{sq} \hat{i}_{sd} - \hat{v}_{sd} \hat{i}_{sq} \\ &= L_{ks} \dot{\theta}_s \left(\hat{i}_{sd}^2 + \hat{i}_{sq}^2 \right) + M \hat{i}_{sd}^2 \dot{\theta}_s \end{aligned} \tag{9}$$

Eq. (8) is directly derived from the Eq. (1), while (9) can be obtained rearranging Eq. (1) in steady state conditions and remembering that $\dot{\theta}_s = \dot{\theta}_r + \dot{\theta}$. All the adjustable models depend on R_r, since $\hat{i}_{sd,q}$ are related to the d,q axes position, which is associated to the estimated rotor flux space vector position $\hat{\theta}_s(\hat{R}_r)$ (see Fig. 2). Furthermore, $\hat{T}$ depends on estimated rotor flux magnitude $\hat{\psi}_r(\hat{R}_r)$.

4. Sensitivity analysis

In this section the main results of the sensitivity analyses for the proposed methods are summarized. For the reactive power approach, the sensitivity analysis is directly based on mathematical definition of Q. Vice-versa, for the torque indicator, the analysis is obtained with the aid of a "sensitivity transfer function" (*STF*), defined as the ratio between the estimated rotor flux phasor (based on estimated rotor resistance) and the real one (based on the real rotor resistance). The sensitivity analyses have been performed for different rotor resistance errors, under different load torque conditions (expressed by means of different slip speed) and speeds.

In order to obtain numerical results, the motor used for the traction of a prototype of an electric commercial vehicle, developed in the Mechanical Department of the Politecnico di Milano, has been considered [27]. The motor adopted for simulation and experimentation is a four poles 180 V 40 kW/70 kW rated/max power induction motor. Table 1 reports the motor parameters. In simulation, the "per unit" approach has been adopted in order to generalize results to different IMs.

4.1. Reactive power method

As reported in [24], starting from the equivalent circuit of the IM model in steady-state conditions shown in Fig. 3, it is possible to obtain the reactive power error.

If the total motor impedance is expressed as a function of the motor parameters and angular frequency, both for the proper rotor

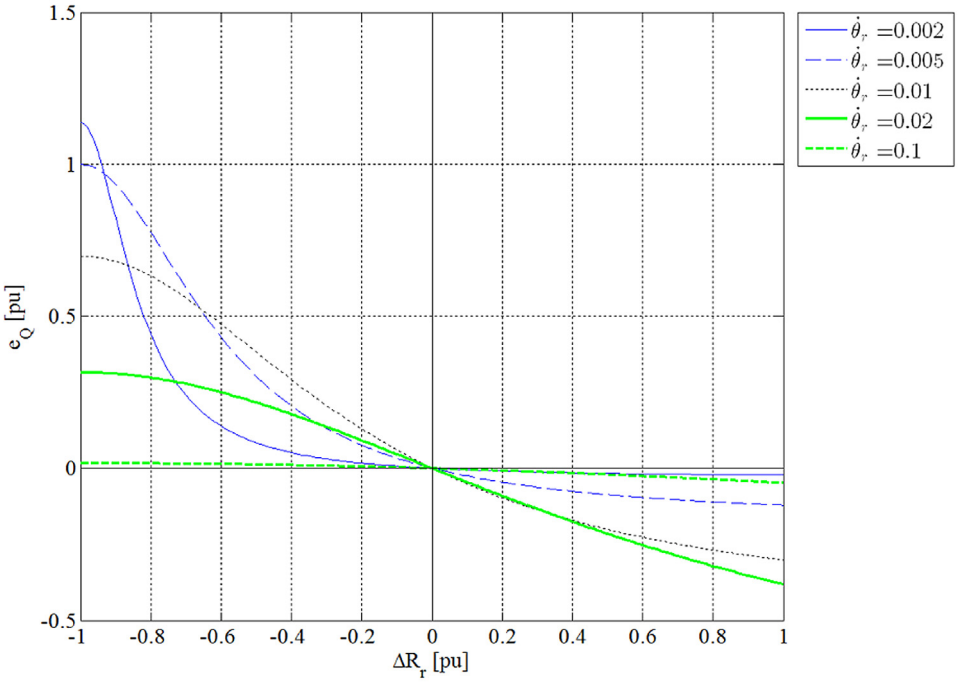

Fig. 4. e_Q trend related to ΔR_{r_pu} and absolute rotor slip speed.

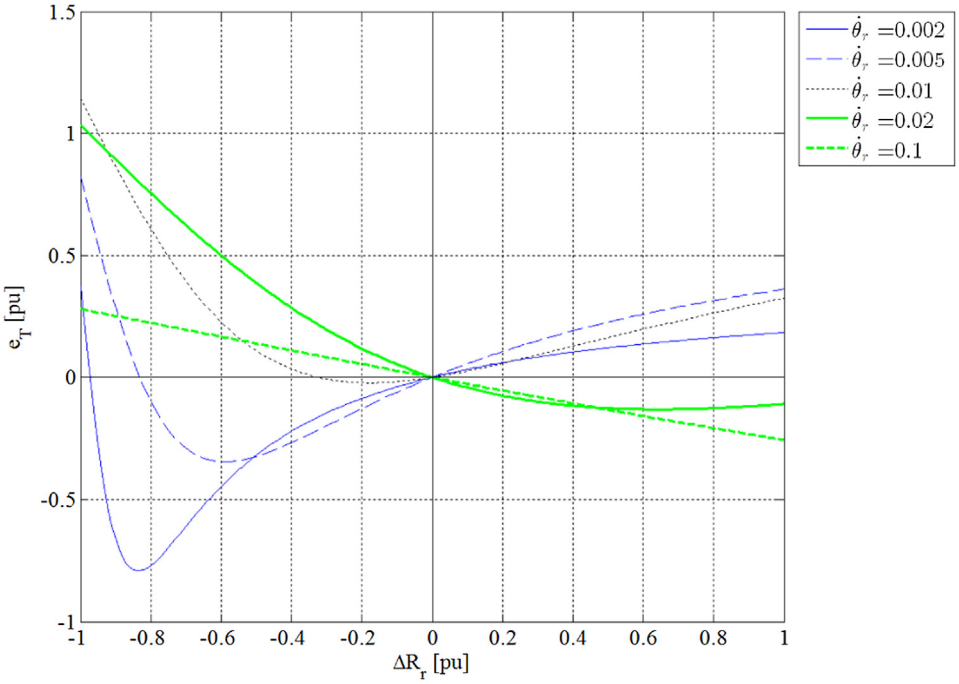

Fig. 5. e_T trend related to ΔR_{r_pu} and absolute rotor slip speed.

resistance value R_r and the estimated one $\hat{R}_r$, the Eq. (10) can be obtained.

$$\begin{cases} Z = R_s + j\dot{\theta}_s L_{ks} + \dfrac{j\dot{\theta}_s M R_r}{j\dot{\theta}_r M + R_r} \\ \hat{Z} = R_s + j\dot{\theta}_s L_{ks} + \dfrac{j\dot{\theta}_s M \hat{R}_r}{j\dot{\theta}_r M + \hat{R}_r} \end{cases} \tag{10}$$

Since the reactive power can be expressed as $\Im\left(Z \cdot \bar{i}_s \cdot \underline{i}^s\right)$, an error index e_Q, based on reactive power, can be identified as in (11).

$$e_Q = \frac{Q - \hat{Q}}{|\bar{i}_s|^2} = \frac{\Im\left(Z \cdot \bar{i}_s \cdot \underline{i}^s\right) - \Im\left(\hat{Z} \cdot \bar{i}_s \cdot \underline{i}^s\right)}{|\bar{i}_s|^2} = \Im(Z) - \Im\left(\hat{Z}\right) \tag{11}$$

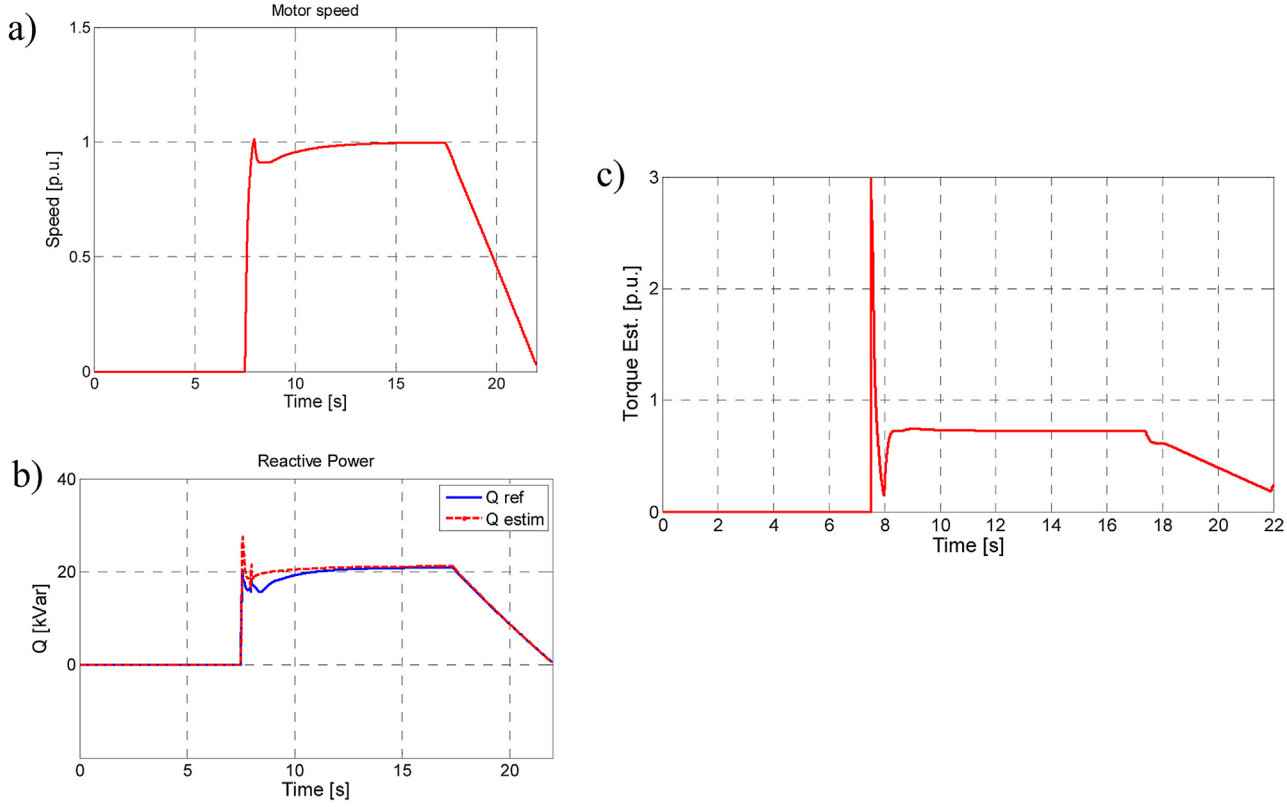

Fig. 6. Motor speed (a), reactive power (b) and torque (c) for $\hat{R}_r > R_r$.

Considering together (11) and t(10), the expression reported in (12) can be obtained.

$$e_Q = \frac{Q - \hat{Q}}{|\bar{i}_s|^2} = \left(\frac{MR_r^2}{R_r^2 + \left(\dot{\theta}_r M\right)^2} - \frac{M\hat{R}_r^2}{\hat{R}_r^2 + \left(\dot{\theta}_r M\right)^2} \right) \dot{\theta}_s \tag{12}$$

The variables stated in (13) are also defined.

$$\begin{cases} \hat{R}_r = R_r + \Delta R_r \\ \Delta R_{r\_pu} = \dfrac{\Delta R_r}{R_r} \end{cases} \tag{13}$$

Fig. 4 shows the trend of e_Q as a function of the rotor resistance error ΔR_{r_pu} and the absolute slip velocity $\dot{\theta}_r$, for a motor speed equal to 0.5 p.u. The analysis has been performed in the whole speed range, but, since a "per unit" approach has been adopted, plots are quite similar. It is possible to notice that this indicator has a nonlinear behavior. Nevertheless, there is a particularly simple relation between the sign of the error e_Q and the sign of the rotor resistance error ΔR_{r_pu} for all the slip speed values.

This relation can be used to define the correction algorithm. In fact, a positive reactive power error means that ΔR_{r_pu} is negative. It denotes that the estimated value of rotor resistance is less than the real one and it has to be increased by the correction algorithm. Vice-versa, a negative reactive power error is associated to a positive ΔR_{r_pu}, thus the estimated value of rotor resistance has to be decreased by the correction algorithm. Moreover, this indicator is independent of the sign of the slip speed $\dot{\theta}_r$, as reported in (12).

4.2. Torque method

As mentioned above, the position of the d-q reference frame θ_s is unknown and can only be calculated using an estimator. If the estimated position $\hat{\theta}_s$ differs from the real one θ_s, the estimated phasor $\hat{\bar{\psi}}_r$ differs from the real one $\bar{\psi}_r$ too, both in magnitude and angular position. It is possible to describe the estimation error using a "sensitivity transfer function" (*STF*). In order to obtain the proper transfer function, the rotor flux space vector can be conveniently described in the stator reference frame, as reported in (14) [25]. Rearranging the equations of the model (14), it is possible to define the real and estimated flux space vectors.

$$\begin{cases} 0 = R_r \bar{i}_r + p\bar{\psi}_r - j\dot{\theta}\bar{\psi}_r \\ \bar{\psi}_r = M(\bar{i}_s + \bar{i}_r) \end{cases} \tag{14}$$

Considering that in steady state condition the derivative operator p can be assumed to be equal to $j\dot{\theta}_s$, the magnitude and the angle of the *STF* can be defined as reported in (15). It is possible to notice that they are R_r and $\dot{\theta}_r$ dependent.

$$\begin{aligned} |STF| &= \left|\frac{\hat{\bar{\psi}}_r}{\bar{\psi}_r}\right| = \left(1 + \Delta R_{r\_pu}\right) \sqrt{\frac{1 + \left(\dfrac{M}{R_r}\dot{\theta}_r\right)^2}{\left(1 + \Delta R_{r\_pu}\right)^2 + \left(\dfrac{M}{R_r}\dot{\theta}_r\right)^2}} \\ \angle STF &= \angle \frac{\hat{\bar{\psi}}_r}{\bar{\psi}_r} = \varepsilon = tg^{-1}\left(\frac{M}{R_r}\dot{\theta}_r\right) - tg^{-1}\left(\frac{\dfrac{M}{R_r}\dot{\theta}_r}{\left(1 + \Delta R_{r\_pu}\right)}\right) \end{aligned} \tag{15}$$

The torque error is defined in (16), where estimated rotor flux magnitude and position can be rearranged as a function of the *STF*, as reported in (17) (see also Fig. 2).

$$\begin{aligned} e_T &= \frac{T - \hat{T}}{|\bar{i}_s|} = n|\bar{\psi}_r| \cdot \sin\gamma - n|\hat{\bar{\psi}}_r| \cdot \sin\hat{\gamma} \\ &= n\left[|\bar{\psi}_r| \cdot \sin\gamma - |\hat{\bar{\psi}}_r| \cdot \sin\hat{\gamma}\right] \end{aligned} \tag{16}$$

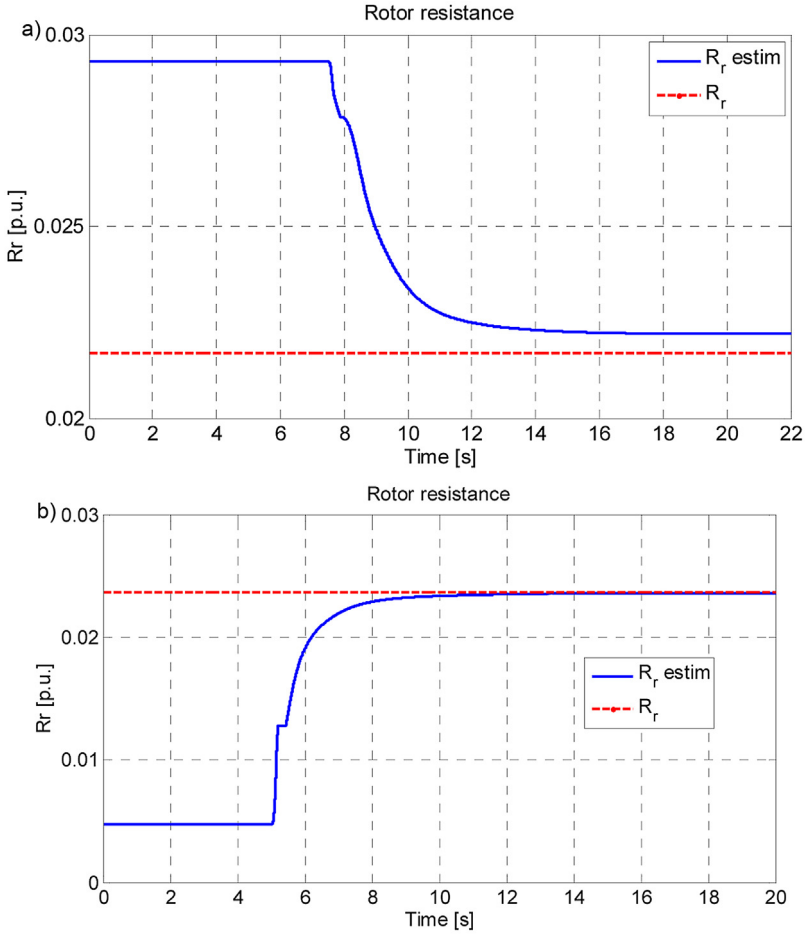

Fig. 7. $\hat{R}_r$ correction algorithm behavior for the reactive power indicators (a) for $\hat{R}_r > R_r$ (b) for $\hat{R}_r < R_r$.

$$\begin{cases} \hat{\gamma} = \gamma - \varepsilon = \gamma - \angle STF \\ |\hat{\bar{\psi}}_r| = |STF| \cdot |\bar{\psi}_r| \end{cases} \tag{17}$$

In this way, the torque error can be analyzed as a function of the rotor resistance variations and the absolute slip speed $\dot{\theta}_r$. For example, the diagram reported in Fig. 5 can be obtained evaluating the torque indicator for a speed corresponding to a 0.5 p.u of the nominal one. Also in this case, the analysis has been performed in the whole speed range, obtaining quite similar plots. It is possible to notice that this indicator has a nonlinear behavior. In fact, the sign of the error e_T is not homogeneous with the sign of the rotor resistance error for some slip speeds. Furthermore, the trend is not monotonic for absolute slips less than a certain amount of the rated speed.

This threshold value is independent of the motor speed, but is a function of motor parameters, as it is possible to notice looking at the expressions of the magnitude and the angle of the *STF* reported in (15). For example, for the considered motor, it is equal to 0.01 p.u. Moreover, from (15), it is also possible to notice that this indicator is dependent on the sign of the slip speed. These considerations can be used to drive the correction algorithm, which has to be activated only for slip speeds (hence the torque) greater than a threshold and only for positive speeds (traction condition).

4.3. Summary of results

Considering the analysis results previously presented, it is possible to define pros and cons for each indicator.

For the reactive power indicator, the following advantages can be pointed out:

- for all the slip and speed values, there is a simple relation between e_Q and ΔR_{r_pu} (see Fig. 4);
- e_Q is independent on the sign of the slip (see (12)).

The main drawback is that the adjustable model (9), used in MRAS approach, directly depends on M and L_{ks} parameters.

For the torque indicator the following advantages can be pointed out:

- the sign of e_T is related to the sign of ΔR_{r_pu} and the trend is monotonic when the absolute slip is larger than a threshold (see Fig. 5);
- the slip threshold is related only to the motor data, so it is constant for different speeds (see (15)).

The main drawbacks are:

- when the absolute slip is smaller than the threshold, the trend of e_T is not monotonic (see Fig. 5);
- e_T is related to the sign of the slip (see (15));
- the value of the rotor flux, used in MRAS model (5), is obtained by a low-pass first-order filter instead of the theoretical pure integrator, so the calculated values are correct only for speeds larger than the cut-off frequency of the filter;
- the value of the rotor flux, used in MRAS model (5), depends also on R_s, see (7).

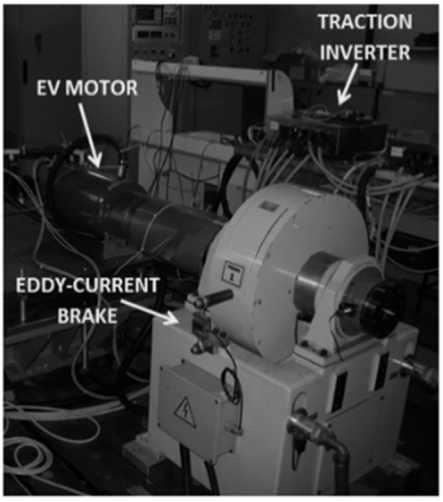

Fig. 8. Laboratory experimental set up.

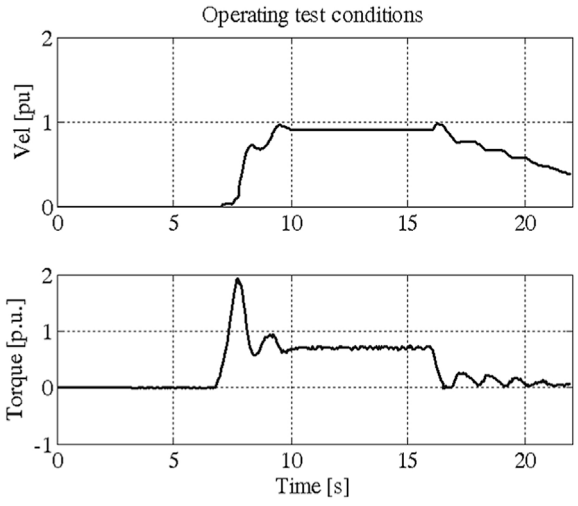

Fig. 9. Motor speed and torque during a step transient operation with $\hat{R}_r$ initially set greater than R_r.

5. Simulation results

A Matlab/Simulink simulation model [25] has been developed to test the R_r correction algorithm feasibility under dynamic conditions. Only the simulation results obtained for the reactive power based R_r estimation algorithm have been reported here since it is the most promising one. Simulation results, regarding the torque indicator, are available in Ref. [24].

The estimation algorithm includes also these rules:

- the algorithm is activated only for motoring condition (no correction during regenerative braking);
- the algorithm is activated when speed is greater than the threshold value (0.1 p.u.);
- a 2% dead-zone around the error value is implemented; in this way, there is no correction if the indicator error e_Q is less than 2%.
- The correction law is a simple integrator, therefore if the error is positive, $\hat{R}_r$ is increased and vice versa.
- the integral gain of the correction law is intentionally set to achieve a slow time response in the $\hat{R}_r$ correction algorithm.

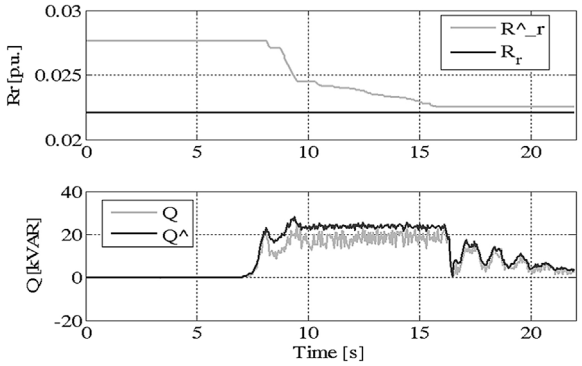

Fig. 10. $\hat{R}_r$ behavior for reactive power indicator—($\hat{R}_r > R_r$).

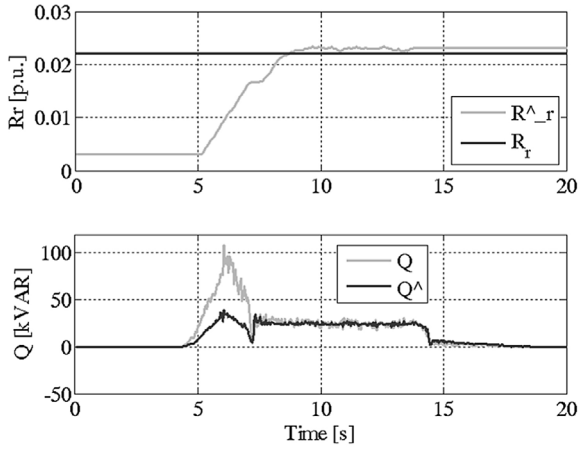

Fig. 11. $\hat{R}_r$ behavior for reactive power indicator—($\hat{R}_r < R_r$).

This simple set of rules has been adopted in order to avoid unstable estimation conditions at very low speed, in which the reference models can also be affected by measuring errors, and under dynamic operating conditions, that are typical in an electric vehicle drive cycle.

The algorithm has been tested applying to the motor acceleration and deceleration transients with timing and loads of a typical EV urban drive cycles.

As an example of the complete system performance, in Fig. 6a the speed step transient response, in Fig. 6b the dynamic behavior of the reactive power estimator and reactive power reference model and in Fig. 6c the estimated torque, when $\hat{R}_r$ is greater than R_r, are reported. The strong oscillations in the first part of the transient, shown in Fig. 6a–c, are due to a wrong R_r parameter set in the simulation model in order to check the algorithm. It is possible to notice that, after about 3 s, the estimated reactive power converges to the real value and the observer works properly. The rotor resistance estimated value $\hat{R}_r$ is converging to the correct value during this time, as it is shown in Fig. 7a.

Fig. 7a and b shows the correction algorithm behavior.

It is possible to notice that the estimation of the rotor resistance converges correctly for an initial value of $\hat{R}_r$, both larger, Fig. 7a and smaller than the real one, Fig. 7b. For the simulation made for testing the algorithm capability to estimate the rotor resistance when the initial condition implies $\hat{R}_r < R_r$, only the resistance behavior during a speed step response is reported in Fig. 7b.

As it is possible to see in Fig. 7, the settling time is around 5 s. Furthermore, in Fig. 7a, it is possible to see a steady state error around 4%, due to the dead-zone rule applied to the error indicator e_Q.

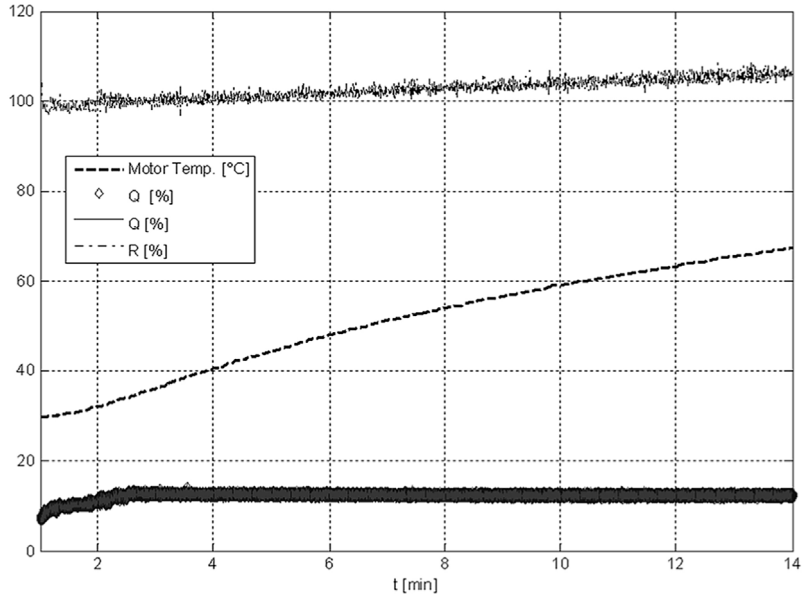

Fig. 12. $\hat{R}_r$ behavior during temperature rise test.

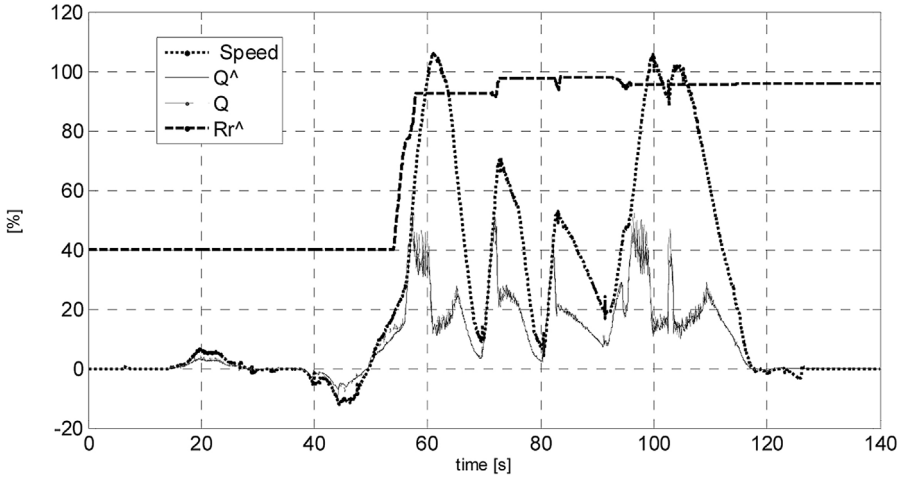

Fig. 13. $\hat{R}_r$ $\hat{R}_r$ adaptation drive test part I.

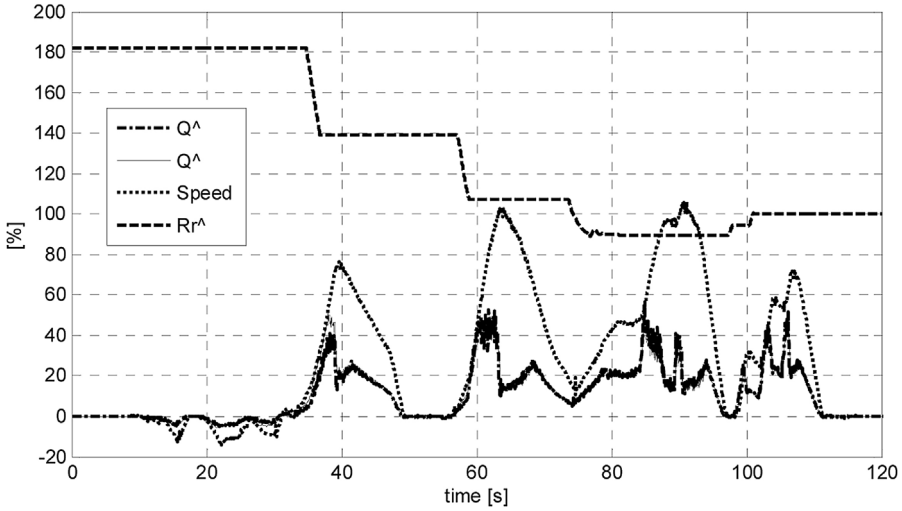

Fig. 14. $\hat{R}_r$ adaptation drive test part II.

6. Test bench experimental results

In order to validate the simulation results previously described, the experimental test set up, shown in Fig. 8, has been used.

It is mainly composed by:

- a water-cooled eddy-current brake, with a rated power of 100 kW and a rated torque of 800 Nm, useful to dynamically change the motor working condition;
- a traction inverter, with a rated input voltage of 300 V dc and a rated output current of 260 A, which implements the FOC algorithm for the control of the motor and the MRAS rotor resistance algorithm;
- the 40/70 kW EV induction motor.

Using this test bench, it is possible to reproduce a typical EV dynamic working in a repeatable way and under safety conditions. For example, Fig. 9 reports a typical motor torque and speed reference step transient response in case of initially estimated rotor resistance set greater than the real one. It is possible to see that the torque has a significant overshoot. This is due to the fact that the state observer is not initially able to correctly estimate the rotor flux modulus and position because the wrong value of the R_r. This generates an incorrect response of the controllers, which produces the reported oscillation. In this situation, the correction algorithm senses a difference between the real R_r value and the one currently used and acts driving the two values to convergence.

In Figs. 10 and 11 the experimental behavior of the correction algorithm is shown.

Analyzing more accurately Fig. 10, it is possible to notice the presence of a negative error (reference model output values are lower than adjustable model ones). This means that the $\hat{R}_r$ value used by the control and estimation algorithms is greater than the real one. So, the correction algorithm has to reduce the $\hat{R}_r$ value. This brings the output values of the adjustable model to converge toward the reference ones and the $\hat{R}_r$ value to converge to the real one. Analyzing Fig. 11, which describes the positive error cases, it is possible to notice that the correction algorithm accurately acts to increase the estimated rotor resistance value.

These results show that the proposed algorithm can properly correct the R_r estimation under different working conditions and with different error indicators.

Comparing the experimental result of Figs. 9–11 with the simulation ones of Figs. 6 and 7, it is possible to see a similar behavior between simulation and experimentation. The noticeable differences are due to the brake system behavior (eddy current brake) on the experimental set-up that is not easy to be modelled.

The algorithm has been also tested during a temperature rising test. The electrical drive has been loaded (rated torque), activated at constant speed (50% of rated speed) and the starting point for $\hat{R}_r$ was set to the correct value. As shown in Fig. 12 the reactive power based MRAS algorithm is able to estimate the rotor resistance while motor temperature is rising. In the heating test, the motor measured temperature rises from 30 °C to 62 °C and the estimated rotor resistance changes of 9%. The plot of Fig. 12 has been scaled as percentage and the rotor resistance is expressed as percentage of the correct value for a clearer understanding. The estimated $\hat{Q}$ and measured reactive power Q are constantly kept equal by the adaptive algorithm.

7. Vehicle based experimental results

The traction electrical drive used on the test bench is equal to the one installed on a plug-in HEV commercial vehicle used for a previous work [27]. The reactive power based MRAS algorithm has been implemented in the control system of the inverter and enabled during an urban drive test. The main tests results are reported in Figs. 13 and 14, where the algorithm capability to find the rotor resistance proper value under dynamic condition are shown. During experiment drive cycle the vehicle driver, through the accelerator pedal, sets the torque reference (*T_ref* in Fig. 1) for the torque loop and the speed is a consequence of vehicle mass, slope, aerodynamic drag, mechanical brakes torque that combining in the vehicle longitudinal dynamics Eq. (4).

In Figs. 13 and 14 the quantities are expressed in percentage of the base values, for a better understanding. In Fig. 13 a first test drive results are shown, where the initial value for $\hat{R}_r$ corresponds to 40% of the correct one. As it is possible to notice, the resistance value rises very quickly to the proper value as soon as the algorithm starts to work (above a certain speed and load with driving torque). Only a residual error is still visible, but it is due to the error dead-band introduced to avoid the continuous adaptation due to the noise and disturbance that are present on the real environment measurement and calculated quantities ($\hat{Q}$ and Q). In Fig. 14 a second test drive results are reported. In this case the initial value for $\hat{R}_r$ corresponds to 180% of the correct one. During the test drive, the estimated rotor resistance converges to the proper R_r value quickly and the reactive power quantities (estimated and measured) assume the same values. This test confirms the validity of the algorithm under dynamic condition in the real application environment.

8. Conclusion

This paper presents an MRAS-based estimation algorithm able to calculate the rotor resistance value of an induction motor working under dynamic conditions. Two different indicators (based on torque and reactive power) have been defined and studied in order to find a set of working conditions under which all the methods have a similar behavior.

These operating conditions have been used as guidelines to identify a unique rotor resistance estimation and correction algorithm. These indicators have been critically analyzed in order to study their sensitivity to load torque, speed and rotor resistance variations and to point out the main advantages and drawbacks of each method. A simple and easy-to implement algorithm has been defined in order to ensure the convergence of the estimation process under dynamic conditions. A set of simulation analysis, referred to typical working conditions for an EV, illustrates that the correction algorithm is able to correctly estimate the real value of R_r, both for initial values larger and smaller than real one, for all the indicators. Therefore, the proposed approaches have been implemented in the Field Oriented Control system of a traction inverter and validated experimentally both on test bench and on vehicle.

Considering the results, the reactive power approach seems to be the most robust method, since its action is independent from torque and speed operating conditions. Additionally, the tests demonstrate that this algorithm is very simple to tune. The proposed algorithm is thus able to estimate the correct value of R_r also in case of wide temperature variation, as experimentally proved. The algorithm is able to work also under dynamic conditions as proved by the experimental drive test performed on the plug-in commercial hybrid vehicle.

References

[1] G. Popa, S. Arsene, M. Mihailescu, Startup railway vehicles with asynchronous traction motors, in: Electrical Systems for Aircraft, Railway and Ship Propulsion, ESARS, Bologna, Italy, 16–18 October, 2012.

[2] Z. Zhu, D. Howe, Electrical machines and drives for electric, hybrid, and fuel cell vehicles, Proc. IEEE 95 (4) (2007) 746–765.

[3] D.G. Dorrell, A.M. Knight, L. Evans, M. Popescu, Analysis and design techniques applied to hybrid vehicle drive machines-assessment of

alternative IPM and induction motor topologies, IEEE Trans. Ind. Electron. 59 (10) (2012) 3690–3699.
[4] F. Cheli, F. Mapelli, R. Manigrasso, D. Tarsitano, Full energetic model of a plugin hybrid electrical vehicle, Power Electronics, Electrical Drives, Automation and Motion, 2008. SPEEDAM 2008. International Symposium on (2008) 733–738.
[5] D. Casadei, M. Mengoni, G. Serra, A. Tani, L. Zarri, M.F. Cabanas, Energy-efficient control of induction motors for automotive applications, 19th International Conference on Electrical Machines, ICEM (2010).
[6] J.W. Finch, D. Giaouris, Controlled AC electrical drives, IEEE Trans. Ind. Electron. 55 (2) (2008) 481–491.
[7] H. Sira-Ramirez, F. Gonzalez-Montanez, J.A. Cortes-Romero, A. Luviano-Juarez, A robust linear field-oriented voltage control for the induction motor: experimental results, IEEE Trans. Ind. Electron. 60 (8) (2013) 3025–3033.
[8] J. Rodríguez, R.M. Kennel, J.R. Espinoza, M. Trincado, C.A. Silva, C.A. Rojas, High-performance control strategies for electrical drives: an experimental assessment, IEEE Trans. Ind. Electron. 59 (2) (2012) 812–820.
[9] X. Yu, M.W. Dunniga, B.W. Williams, A novel rotor resistance identification method for an indirect rotor flux-orientated controlled induction machine system, IEEE Trans. Power Electron. 17 (May (3)) (2002) 353–364.
[10] M. Sharifian, N. Rostami, H. Hatami, Sensorless control of IM based on full-order Luenberger observer: with core loss and rotor resistances estimation, 2010 9th International Power and Energy Conference, IPEC (2010) 567–571.
[11] D.F. Coutinho, L.F.A. Pereira, A robust Luenberger-like observer for induction machines, in: 31 st Annual Conference of IEEE Industrial Electronics Society, IECON, 6–10 November, 2005.
[12] M. Hilairet, F. Auger, E. Berthelot, Speed and rotor flux estimation of induction machines using a two-stage extended Kalman filter, Automatica 45 (8) (2009) 1819–1827.
[13] S. Wade, M.W. Dunnigan, B.W. Williams, Modeling and simulation of induction machine vector control with rotor resistance identification, IEEE Trans. Power Electron. 12 (May (3)) (1997) 495–506.
[14] M. Barut, R. Demir, E. Zerdali, R. Inan, Real-time implementation of bi input-extended Kalman filter-based estimator for speed-sensorless control of induction motors, IEEE Trans. Ind. Electron. 59 (11) (2012) 4197–4206.
[15] Y. Agrebi Zorgani, Y. Koubaa, M. Boussak, Simultaneous estimation of speed and rotor resistance in sensorless ISFOC induction motor drive based on MRAS scheme, in: 19th International Conference on Electrical Machines, ICEM 2010, 6–8 September, 2010.
[16] M. Nandhini Gayathri, S. Himavathi, R. Sankaran, Comparison of rotor flux and reactive power based MRAS rotor resistance estimators for vector controlled induction motor drive, IEEE-International Conference on Advances in Engineering, Science and Management ICAESM-2012 (2012) 183–189.
[17] M. Zerikat, S. Chekroun, A. Mechernene, A robust MRAS-sensorless scheme based rotor and stator resistances estimation of a direct vector controlled induction motor drive, in: 16th International Conference on Methods and Models in Automation and Robotics (MMAR), 22–25 August, 2011, pp. 151–156.
[18] A.V. Ravi Teja, C. Chakraborty, A novel model reference adaptive controller for estimation of speed and stator resistance for vector controlled induction motor drives, in: 2010 IEEE International Symposium on Industrial Electronics (ISIE), 4–7 July, 2010.
[19] A.V. Ravi Teja, C. Chakraborty, S. Maiti, Y. Hori, A new model reference adaptive controller for four quadrant vector controlled induction motor drives, IEEE Trans. Ind. Electron. 59 (October (10)) (2012) 3757–3767.
[20] M.R. Dehbozorgi, H.M. Kojabadi, H. Vahedi, K. Al-Haddad, A comparative study of various MRAS-based IM's rotor resistance adaptation methods, in: IECON 2012—38th Annual Conference on IEEE Industrial Electronics Society, Montreal, 25–28 October, 2012, pp. 4070–4075.
[21] B.M. Chandra, S.T. Kalyani, Online identification and adaptation of rotor resistance in feedforward vector controlled induction motor drive, in: IEEE 5th India International Conference on Power Electronics (IICPE), 6–8 December, 2012, pp. 1–6.
[22] B. Karanayil, M.F. Rahman, C. Grantham, Online stator and rotor resistance estimation scheme using artificial neural networks for vector controlled speed sensorless induction motor drive, IEEE Trans. Ind. Electron. 54 (1) (2007) 167–176.
[23] S. Maiti, V. Verma, C. Chakraborty, Y. Hori, An adaptive speed sensorless induction motor drive with artificial neural network for stability enhancement, IEEE Trans. Ind. Inform. 8 (November (4)) (2012) 757–766.
[24] F.L. Mapelli, D. Tarsitano, F. Cheli, A rotor resistance MRAS estimator for EV induction motor traction drive based on torque and reactive stator power: simulation and experimental results, in: Proceedings—2014 International Conference on Electrical Machines, Berlin, Germany ICEM, 2014, pp. 31–37.
[25] F. Mapelli, D. Tarsitano, M. Mauri, Plug-in hybrid electric vehicle: modeling, prototype realization, and inverter losses reduction analysis, IEEE Trans. Ind. Electron. 57 (2) (2010) 598–607.
[26] M. Mauri, F. Mapelli, D. Tarsitano, A reduced losses field oriented control for plug-in hybrid electric vehicle, in: 19th International Conference on Electrical Machines (ICEM), 6–8 Sept., 2010.
[27] F. Mapelli, D. Tarsitano, S. Agostoni, Plug-in hybrid electrical commercial vehicle: modeling and prototype realization, in: Electric Vehicle Conference (IEVC), 2012 Greenville, SC IEEE International, 2012, pp. 1–8.